BABAR-CONF-02/024
SLAC-PUB-9319
hep-ex/0207073
July 2002

Search for the Exclusive Radiative Decays $B \to \rho\gamma$ and $B^0 \to \omega\gamma$

The *BABAR* Collaboration

July 24, 2002

Abstract

A search for the exclusive radiative decays $B \to \rho(770)\gamma$ and $B^0 \to \omega(782)\gamma$ is performed on a sample of 84 million $B\overline{B}$ events collected by the *BABAR* detector at the $PEP-II$ asymmetric e^+e^- collider. No significant signal is seen in any of the channels. We set preliminary upper limits of $\mathcal{B}[B^0 \to \rho^0\gamma] < 1.4 \times 10^{-6}$, $\mathcal{B}[B^+ \to \rho^+\gamma] < 2.3 \times 10^{-6}$ and $\mathcal{B}[B^0 \to \omega\gamma] < 1.2 \times 10^{-6}$ at 90% Confidence Level. Combining these into a single limit on the generic process $B \to \rho\gamma$, we find the preliminary limit $\mathcal{B}[B \to \rho\gamma] < 1.9 \times 10^{-6}$ corresponding, to a limit of $\mathcal{B}[B \to \rho\gamma]/\mathcal{B}[B \to K^*\gamma] < 0.047$ at 90% Confidence Level.

Contributed to the 31^{st} International Conference on High Energy Physics,
7/24—7/31/2002, Amsterdam, The Netherlands

Stanford Linear Accelerator Center, Stanford University, Stanford, CA 94309

Work supported in part by Department of Energy contract DE-AC03-76SF00515.

The *BABAR* Collaboration,

B. Aubert, D. Boutigny, J.-M. Gaillard, A. Hicheur, Y. Karyotakis, J. P. Lees, P. Robbe, V. Tisserand, A. Zghiche

Laboratoire de Physique des Particules, F-74941 Annecy-le-Vieux, France

A. Palano, A. Pompili

Università di Bari, Dipartimento di Fisica and INFN, I-70126 Bari, Italy

J. C. Chen, N. D. Qi, G. Rong, P. Wang, Y. S. Zhu

Institute of High Energy Physics, Beijing 100039, China

G. Eigen, I. Ofte, B. Stugu

University of Bergen, Inst. of Physics, N-5007 Bergen, Norway

G. S. Abrams, A. W. Borgland, A. B. Breon, D. N. Brown, J. Button-Shafer, R. N. Cahn, E. Charles, M. S. Gill, A. V. Gritsan, Y. Groysman, R. G. Jacobsen, R. W. Kadel, J. Kadyk, L. T. Kerth, Yu. G. Kolomensky, J. F. Kral, C. LeClerc, M. E. Levi, G. Lynch, L. M. Mir, P. J. Oddone, T. J. Orimoto, M. Pripstein, N. A. Roe, A. Romosan, M. T. Ronan, V. G. Shelkov, A. V. Telnov, W. A. Wenzel

Lawrence Berkeley National Laboratory and University of California, Berkeley, CA 94720, USA

T. J. Harrison, C. M. Hawkes, D. J. Knowles, S. W. O'Neale, R. C. Penny, A. T. Watson, N. K. Watson

University of Birmingham, Birmingham, B15 2TT, United Kingdom

T. Deppermann, K. Goetzen, H. Koch, B. Lewandowski, K. Peters, H. Schmuecker, M. Steinke

Ruhr Universität Bochum, Institut für Experimentalphysik 1, D-44780 Bochum, Germany

N. R. Barlow, W. Bhimji, J. T. Boyd, N. Chevalier, P. J. Clark, W. N. Cottingham, C. Mackay, F. F. Wilson

University of Bristol, Bristol BS8 1TL, United Kingdom

K. Abe, C. Hearty, T. S. Mattison, J. A. McKenna, D. Thiessen

University of British Columbia, Vancouver, BC, Canada V6T 1Z1

S. Jolly, A. K. McKemey

Brunel University, Uxbridge, Middlesex UB8 3PH, United Kingdom

V. E. Blinov, A. D. Bukin, A. R. Buzykaev, V. B. Golubev, V. N. Ivanchenko, A. A. Korol, E. A. Kravchenko, A. P. Onuchin, S. I. Serednyakov, Yu. I. Skovpen, A. N. Yushkov

Budker Institute of Nuclear Physics, Novosibirsk 630090, Russia

D. Best, M. Chao, D. Kirkby, A. J. Lankford, M. Mandelkern, S. McMahon, D. P. Stoker

University of California at Irvine, Irvine, CA 92697, USA

C. Buchanan, S. Chun

University of California at Los Angeles, Los Angeles, CA 90024, USA

H. K. Hadavand, E. J. Hill, D. B. MacFarlane, H. Paar, S. Prell, Sh. Rahatlou, G. Raven, U. Schwanke, V. Sharma

University of California at San Diego, La Jolla, CA 92093, USA

J. W. Berryhill, C. Campagnari, B. Dahmes, P. A. Hart, N. Kuznetsova, S. L. Levy, O. Long, A. Lu, M. A. Mazur, J. D. Richman, W. Verkerke

University of California at Santa Barbara, Santa Barbara, CA 93106, USA

J. Beringer, A. M. Eisner, M. Grothe, C. A. Heusch, W. S. Lockman, T. Pulliam, T. Schalk, R. E. Schmitz, B. A. Schumm, A. Seiden, M. Turri, W. Walkowiak, D. C. Williams, M. G. Wilson

University of California at Santa Cruz, Institute for Particle Physics, Santa Cruz, CA 95064, USA

E. Chen, G. P. Dubois-Felsmann, A. Dvoretskii, D. G. Hitlin, F. C. Porter, A. Ryd, A. Samuel, S. Yang

California Institute of Technology, Pasadena, CA 91125, USA

S. Jayatilleke, G. Mancinelli, B. T. Meadows, M. D. Sokoloff

University of Cincinnati, Cincinnati, OH 45221, USA

T. Barillari, P. Bloom, W. T. Ford, U. Nauenberg, A. Olivas, P. Rankin, J. Roy, J. G. Smith, W. C. van Hoek, L. Zhang

University of Colorado, Boulder, CO 80309, USA

J. L. Harton, T. Hu, M. Krishnamurthy, A. Soffer, W. H. Toki, R. J. Wilson, J. Zhang

Colorado State University, Fort Collins, CO 80523, USA

D. Altenburg, T. Brandt, J. Brose, T. Colberg, M. Dickopp, R. S. Dubitzky, A. Hauke, E. Maly, R. Müller-Pfefferkorn, S. Otto, K. R. Schubert, R. Schwierz, B. Spaan, L. Wilden

Technische Universität Dresden, Institut für Kern- und Teilchenphysik, D-01062 Dresden, Germany

D. Bernard, G. R. Bonneaud, F. Brochard, J. Cohen-Tanugi, S. Ferrag, S. T'Jampens, Ch. Thiebaux, G. Vasileiadis, M. Verderi

Ecole Polytechnique, LLR, F-91128 Palaiseau, France

A. Anjomshoaa, R. Bernet, A. Khan, D. Lavin, F. Muheim, S. Playfer, J. E. Swain, J. Tinslay

University of Edinburgh, Edinburgh EH9 3JZ, United Kingdom

M. Falbo

Elon University, Elon University, NC 27244-2010, USA

C. Borean, C. Bozzi, L. Piemontese, A. Sarti

Università di Ferrara, Dipartimento di Fisica and INFN, I-44100 Ferrara, Italy

E. Treadwell

Florida A&M University, Tallahassee, FL 32307, USA

F. Anulli,[1] R. Baldini-Ferroli, A. Calcaterra, R. de Sangro, D. Falciai, G. Finocchiaro, P. Patteri, I. M. Peruzzi,[1] M. Piccolo, A. Zallo

Laboratori Nazionali di Frascati dell'INFN, I-00044 Frascati, Italy

S. Bagnasco, A. Buzzo, R. Contri, G. Crosetti, M. Lo Vetere, M. Macri, M. R. Monge, S. Passaggio, F. C. Pastore, C. Patrignani, E. Robutti, A. Santroni, S. Tosi

Università di Genova, Dipartimento di Fisica and INFN, I-16146 Genova, Italy

[1]Also with Università di Perugia, I-06100 Perugia, Italy

S. Bailey, M. Morii

Harvard University, Cambridge, MA 02138, USA

R. Bartoldus, G. J. Grenier, U. Mallik

University of Iowa, Iowa City, IA 52242, USA

J. Cochran, H. B. Crawley, J. Lamsa, W. T. Meyer, E. I. Rosenberg, J. Yi

Iowa State University, Ames, IA 50011-3160, USA

M. Davier, G. Grosdidier, A. Höcker, H. M. Lacker, S. Laplace, F. Le Diberder, V. Lepeltier, A. M. Lutz, T. C. Petersen, S. Plaszczynski, M. H. Schune, L. Tantot, S. Trincaz-Duvoid, G. Wormser

Laboratoire de l'Accélérateur Linéaire, F-91898 Orsay, France

R. M. Bionta, V. Brigljević , D. J. Lange, K. van Bibber, D. M. Wright

Lawrence Livermore National Laboratory, Livermore, CA 94550, USA

A. J. Bevan, J. R. Fry, E. Gabathuler, R. Gamet, M. George, M. Kay, D. J. Payne, R. J. Sloane, C. Touramanis

University of Liverpool, Liverpool L69 3BX, United Kingdom

M. L. Aspinwall, D. A. Bowerman, P. D. Dauncey, U. Egede, I. Eschrich, G. W. Morton, J. A. Nash, P. Sanders, D. Smith, G. P. Taylor

University of London, Imperial College, London, SW7 2BW, United Kingdom

J. J. Back, G. Bellodi, P. Dixon, P. F. Harrison, R. J. L. Potter, H. W. Shorthouse, P. Strother, P. B. Vidal

Queen Mary, University of London, E1 4NS, United Kingdom

G. Cowan, H. U. Flaecher, S. George, M. G. Green, A. Kurup, C. E. Marker, T. R. McMahon, S. Ricciardi, F. Salvatore, G. Vaitsas, M. A. Winter

University of London, Royal Holloway and Bedford New College, Egham, Surrey TW20 0EX, United Kingdom

D. Brown, C. L. Davis

University of Louisville, Louisville, KY 40292, USA

J. Allison, R. J. Barlow, A. C. Forti, F. Jackson, G. D. Lafferty, A. J. Lyon, N. Savvas, J. H. Weatherall, J. C. Williams

University of Manchester, Manchester M13 9PL, United Kingdom

A. Farbin, A. Jawahery, V. Lillard, D. A. Roberts, J. R. Schieck

University of Maryland, College Park, MD 20742, USA

G. Blaylock, C. Dallapiccola, K. T. Flood, S. S. Hertzbach, R. Kofler, V. B. Koptchev, T. B. Moore, H. Staengle, S. Willocq

University of Massachusetts, Amherst, MA 01003, USA

B. Brau, R. Cowan, G. Sciolla, F. Taylor, R. K. Yamamoto

Massachusetts Institute of Technology, Laboratory for Nuclear Science, Cambridge, MA 02139, USA

M. Milek, P. M. Patel

McGill University, Montréal, QC, Canada H3A 2T8

F. Palombo

Università di Milano, Dipartimento di Fisica and INFN, I-20133 Milano, Italy

J. M. Bauer, L. Cremaldi, V. Eschenburg, R. Kroeger, J. Reidy, D. A. Sanders, D. J. Summers

University of Mississippi, University, MS 38677, USA

C. Hast, P. Taras

Université de Montréal, Laboratoire René J. A. Lévesque, Montréal, QC, Canada H3C 3J7

H. Nicholson

Mount Holyoke College, South Hadley, MA 01075, USA

C. Cartaro, N. Cavallo, G. De Nardo, F. Fabozzi, C. Gatto, L. Lista, P. Paolucci, D. Piccolo, C. Sciacca

Università di Napoli Federico II, Dipartimento di Scienze Fisiche and INFN, I-80126, Napoli, Italy

J. M. LoSecco

University of Notre Dame, Notre Dame, IN 46556, USA

J. R. G. Alsmiller, T. A. Gabriel

Oak Ridge National Laboratory, Oak Ridge, TN 37831, USA

J. Brau, R. Frey, M. Iwasaki, C. T. Potter, N. B. Sinev, D. Strom, E. Torrence

University of Oregon, Eugene, OR 97403, USA

F. Colecchia, A. Dorigo, F. Galeazzi, M. Margoni, M. Morandin, M. Posocco, M. Rotondo, F. Simonetto, R. Stroili, C. Voci

Università di Padova, Dipartimento di Fisica and INFN, I-35131 Padova, Italy

M. Benayoun, H. Briand, J. Chauveau, P. David, Ch. de la Vaissière, L. Del Buono, O. Hamon, Ph. Leruste, J. Ocariz, M. Pivk, L. Roos, J. Stark

Universités Paris VI et VII, Lab de Physique Nucléaire H. E., F-75252 Paris, France

P. F. Manfredi, V. Re, V. Speziali

Università di Pavia, Dipartimento di Elettronica and INFN, I-27100 Pavia, Italy

L. Gladney, Q. H. Guo, J. Panetta

University of Pennsylvania, Philadelphia, PA 19104, USA

C. Angelini, G. Batignani, S. Bettarini, M. Bondioli, F. Bucci, G. Calderini, E. Campagna, M. Carpinelli, F. Forti, M. A. Giorgi, A. Lusiani, G. Marchiori, F. Martinez-Vidal, M. Morganti, N. Neri, E. Paoloni, M. Rama, G. Rizzo, F. Sandrelli, G. Triggiani, J. Walsh

Università di Pisa, Scuola Normale Superiore and INFN, I-56010 Pisa, Italy

M. Haire, D. Judd, K. Paick, L. Turnbull, D. E. Wagoner

Prairie View A&M University, Prairie View, TX 77446, USA

J. Albert, G. Cavoto,[2] N. Danielson, P. Elmer, C. Lu, V. Miftakov, J. Olsen, S. F. Schaffner, A. J. S. Smith, A. Tumanov, E. W. Varnes

Princeton University, Princeton, NJ 08544, USA

[2]Also with Università di Roma La Sapienza, Roma, Italy

F. Bellini, D. del Re, R. Faccini,[3] F. Ferrarotto, F. Ferroni, E. Leonardi, M. A. Mazzoni, S. Morganti, G. Piredda, F. Safai Tehrani, M. Serra, C. Voena

Università di Roma La Sapienza, Dipartimento di Fisica and INFN, I-00185 Roma, Italy

S. Christ, G. Wagner, R. Waldi

Universität Rostock, D-18051 Rostock, Germany

T. Adye, N. De Groot, B. Franek, N. I. Geddes, G. P. Gopal, S. M. Xella

Rutherford Appleton Laboratory, Chilton, Didcot, Oxon, OX11 0QX, United Kingdom

R. Aleksan, S. Emery, A. Gaidot, P.-F. Giraud, G. Hamel de Monchenault, W. Kozanecki, M. Langer, G. W. London, B. Mayer, G. Schott, B. Serfass, G. Vasseur, Ch. Yeche, M. Zito

DAPNIA, Commissariat à l'Energie Atomique/Saclay, F-91191 Gif-sur-Yvette, France

M. V. Purohit, A. W. Weidemann, F. X. Yumiceva

University of South Carolina, Columbia, SC 29208, USA

I. Adam, D. Aston, N. Berger, A. M. Boyarski, M. R. Convery, D. P. Coupal, D. Dong, J. Dorfan, W. Dunwoodie, R. C. Field, T. Glanzman, S. J. Gowdy, E. Grauges , T. Haas, T. Hadig, V. Halyo, T. Himel, T. Hryn'ova, M. E. Huffer, W. R. Innes, C. P. Jessop, M. H. Kelsey, P. Kim, M. L. Kocian, U. Langenegger, D. W. G. S. Leith, S. Luitz, V. Luth, H. L. Lynch, H. Marsiske, S. Menke, R. Messner, D. R. Muller, C. P. O'Grady, V. E. Ozcan, A. Perazzo, M. Perl, S. Petrak, H. Quinn, B. N. Ratcliff, S. H. Robertson, A. Roodman, A. A. Salnikov, T. Schietinger, R. H. Schindler, J. Schwiening, G. Simi, A. Snyder, A. Soha, S. M. Spanier, J. Stelzer, D. Su, M. K. Sullivan, H. A. Tanaka, J. Va'vra, S. R. Wagner, M. Weaver, A. J. R. Weinstein, W. J. Wisniewski, D. H. Wright, C. C. Young

Stanford Linear Accelerator Center, Stanford, CA 94309, USA

P. R. Burchat, C. H. Cheng, T. I. Meyer, C. Roat

Stanford University, Stanford, CA 94305-4060, USA

R. Henderson

TRIUMF, Vancouver, BC, Canada V6T 2A3

W. Bugg, H. Cohn

University of Tennessee, Knoxville, TN 37996, USA

J. M. Izen, I. Kitayama, X. C. Lou

University of Texas at Dallas, Richardson, TX 75083, USA

F. Bianchi, M. Bona, D. Gamba

Università di Torino, Dipartimento di Fisica Sperimentale and INFN, I-10125 Torino, Italy

L. Bosisio, G. Della Ricca, S. Dittongo, L. Lanceri, P. Poropat, L. Vitale, G. Vuagnin

Università di Trieste, Dipartimento di Fisica and INFN, I-34127 Trieste, Italy

R. S. Panvini

Vanderbilt University, Nashville, TN 37235, USA

[3]Also with University of California at San Diego, La Jolla, CA 92093, USA

S. W. Banerjee, C. M. Brown, D. Fortin, P. D. Jackson, R. Kowalewski, J. M. Roney

University of Victoria, Victoria, BC, Canada V8W 3P6

H. R. Band, S. Dasu, M. Datta, A. M. Eichenbaum, H. Hu, J. R. Johnson, R. Liu, F. Di Lodovico, A. Mohapatra, Y. Pan, R. Prepost, I. J. Scott, S. J. Sekula, J. H. von Wimmersperg-Toeller, J. Wu, S. L. Wu, Z. Yu

University of Wisconsin, Madison, WI 53706, USA

H. Neal

Yale University, New Haven, CT 06511, USA

1 Introduction

The effective flavor-changing neutral current processes $B \to \rho\gamma$ and $B^0 \to \omega\gamma$ probe physics at high mass scales both within the Standard Model and within the context of possible new physics scenarios through the underlying $b \to d\gamma$ "penguin" transition [1]. The decays are analogous to the $B \to K^*\gamma$ process mediated by the $b \to s\gamma$ transition. The expected rate of $b \to d\gamma$ transitions is suppressed by the ratio of CKM matrix elements $|V_{td}/V_{ts}|^2$ relative to $b \to s\gamma$ transitions. There has been considerable interest recently in these exclusive channels, resulting in several calculations of the branching fractions expected in the Standard Model, which indicate a range $\mathcal{B}[B^+ \to \rho^+\gamma] = (0.9 - 1.5) \times 10^{-6}$ [2]. Though the theoretical uncertainties for the branching fractions remain large, the possibility of extracting the ratio of CKM elements $|V_{td}/V_{ts}|^2$ through the ratio $\mathcal{B}[B \to (\rho/\omega)\gamma]/\mathcal{B}[B \to K^*\gamma]$ with less uncertainty has been explored [3][4]. The observation of $B \to \rho\gamma$ and $B^0 \to \omega\gamma$ would constitute the first evidence of the $b \to d\gamma$ radiative transition and is of considerable interest as the first step towards extracting $|V_{td}/V_{ts}|$ from measurements of these channels. Previous searches have found no evidence for these decays [5].

2 The *BABAR* Detector and Dataset

The decay $B \to \rho\gamma$ is reconstructed in the modes $B^0 \to \rho^0\gamma$ with $\rho^0 \to \pi^+\pi^-$ and $B^+ \to \rho^+\gamma$ with $\rho^+ \to \pi^+\pi^0$ (charge-conjugate modes are implied throughout), while $B^0 \to \omega\gamma$ is reconstructed with $\omega \to \pi^+\pi^-\pi^0$. The analysis uses a sample of 84 million $B\overline{B}$ events in $78\,\mathrm{fb}^{-1}$ of data collected by the *BABAR* detector [6] at the $PEP-II$ collider [7] on the $\Upsilon(4S)$ resonance ("on-resonance"), and $9.6\,\mathrm{fb}^{-1}$ of data taken $40\,\mathrm{MeV}/c^2$ below the $\Upsilon(4S)$ resonance ("off-resonance"). The reconstruction uses quantities both in the laboratory and $\Upsilon(4S)$ center-of-mass (CMS) frames, where the latter are denoted by an asterisk. The detector response to the signal and background processes are studied with a detailed Monte Carlo simulation based on Geant4 [8] and cross-checked with control samples in the data. The off-resonance data provide a control sample of the primary backgrounds from the continuum production of u, d, s, and c quark-antiquark pairs, while exclusively reconstructed $B \to D\pi$ decays provide a sample to cross-check the simulation of $B\overline{B}$ events.

3 Analysis Method

3.1 Reconstruction of the Primary Photon

The primary photon in the decay is identified as a local maximum within a contiguous deposition of energy in the crystal array of the electromagnetic calorimeter (EMC). We require that the photon lies in the calorimeter acceptance of $-0.74 < \cos\theta < 0.93$, where θ is the polar angle to the detector axis. The energy of the photon, measured in the center of mass system, must satisfy $1.5 < E^*_\gamma < 3.5$GeV. The photon candidate is required to be isolated from all other local maxima in the calorimeter by 25 cm. It must also be inconsistent with the trajectories of all reconstructed charged tracks. Photons consistent with π^0 and η production are vetoed by removing candidates that form an invariant mass within $20(40)\,\mathrm{MeV}/c^2$ of the $\pi^0(\eta)$ mass when paired with any other photon in the event with energy greater than $50(250)\,\mathrm{MeV}$. Energetic π^0s which produce photons that cannot be resolved as separate local maxima are suppressed by requiring the lateral profile of the energy deposition to be consistent with a single photon.

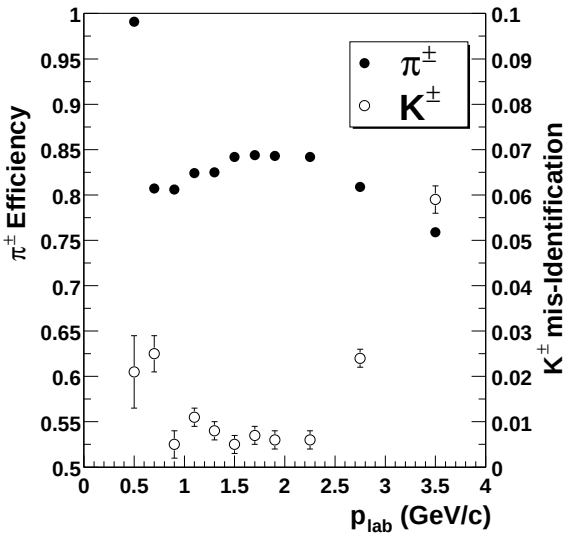

Figure 1: Pion selection performance as measured in data using $D^{*+} \to D^0\pi^+, D^0 \to K^-\pi^+$ decays as a function of momentum in the laboratory frame p_{lab}.

3.2 Reconstruction of Charged Tracks

The charged tracks used in identifying the ρ/ω meson are reconstructed in the silicon vertex detector (SVT) and drift chamber (DCH) and are required to have a trajectory consistent with production near the beam interaction point as well as a minimum of 12 hits in the drift chamber. A charged pion selection based on dE/dx measurements and Cherenkov photons reconstructed in the ring-imaging Cherenkov detector (DIRC) is used to reduce backgrounds from $B \to K^*\gamma$ and other $b \to s\gamma$ processes by vetoing charged kaons from these processes. Both the reconstructed Cherenkov angle and the number of Cherenkov photons observed is required to be consistent with the pion hypothesis. Figure 1 shows the particle identification performance achieved.

3.3 Reconstruction of ρ/ω Meson

The $\rho^0 \to \pi^+\pi^-$ candidates are reconstructed by calculating a common vertex for two tracks of opposite charge. For the $\rho^+ \to \pi^+\pi^0$ and $\omega \to \pi^+\pi^-\pi^0$ reconstruction, π^0 candidates are identified as two photon candidates reconstructed in the calorimeter each of with energy greater than 50 MeV. The invariant mass of the pair is required to be $0.115 < M_{\gamma\gamma} < 0.150\,\mathrm{GeV}/c^2$. A kinematic fit with $M_{\gamma\gamma}$ constrained to the nominal π^0 mass is used to improve the momentum resolution. The ρ^+ candidates result from π^0 candidates paired with an identified charged pion. The invariant mass $M_{\pi\pi}$ of the ρ candidates is required to be between 0.520 and $1.020\,\mathrm{GeV}/c^2$. The ω candidates are reconstructed from combinations of oppositely charged identified pions with a successfully calculated vertex and π^0 candidates with invariant mass $0.7596 < M_{\pi^+\pi^-\pi^0} < 0.8056\,\mathrm{GeV}/c^2$. The momentum of the candidate ρ mesons, measured in the center of mass system must satisfy $2.3 < p^*_\rho < 2.85$ and the ω mesons must satisfy $2.4 < p^*_\omega < 2.8$. This cut, which has very high signal efficiency, is applied in order to reduce the number of events where more than one candidate

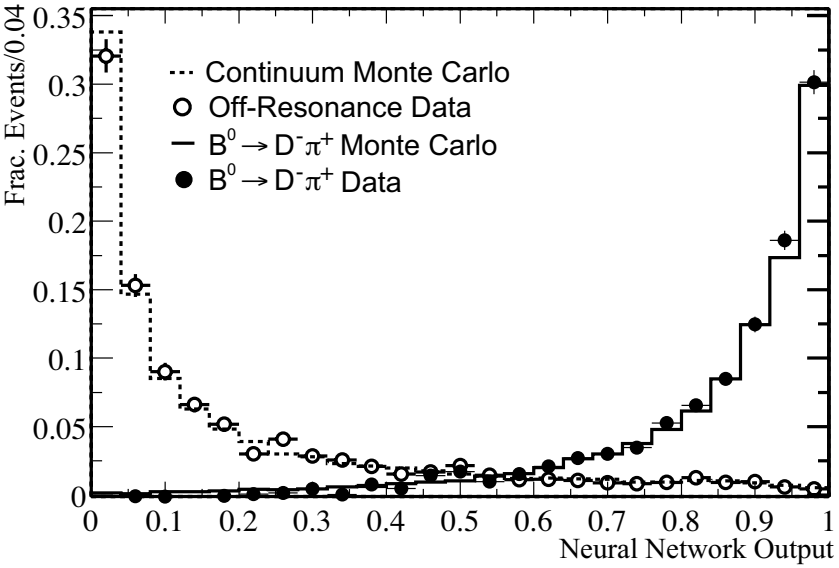

Figure 2: $B^0 \to \rho^0\gamma$ neural network output for Monte Carlo-simulated events with comparison to data control samples.

satisfies all of the cuts.

3.4 Reconstruction of the B Meson

The photon and ρ/ω meson candidate are combined to form the B meson candidate. The kinematic properties of the B meson are evaluated in the CMS using the variables $\Delta E^* = E_B^* - E_{beam}^*$ and the beam-energy substituted mass $m_{\rm ES} = \sqrt{E_{beam}^{*2} - {\rm p}_B'^{*2}}$, where E_{beam}^* is the energy of the beam, $E_B^* = E_\gamma^* + E_{\rho/\omega}^*$ is the reconstructed energy of the B meson candidate and ${\rm p}_B'^*$ is its momentum. For the purposes of the $m_{\rm ES}$ calculation, ${\rm p}_B'^*$ is modified by scaling the photon energy so as to make $E_\gamma^* + E_{\rho/\omega}^* - E_{beam}^* = 0$, under the assumption that the resolution of the primary photon energy dominates the ΔE^* resolution. This procedure reduces the tail in the $m_{\rm ES}$ resolution that results from the asymmetric photon energy response in the EMC. The signal events have $m_{\rm ES} = m_B$ and $\Delta E^* = 0$ up to the experimental resolution of $\sim 3\,{\rm MeV}/c^2$ dominated by the beam-energy spread in the former case, and $\sim 50\,{\rm MeV}$ dominated by the reconstructed photon energy resolution in the latter.

We consider candidates in the region $-0.3 < \Delta E^* < 0.3\,{\rm GeV}$ and $5.2 < m_{\rm ES} < 5.29\,{\rm GeV}/c^2$ and define a signal region of $-0.2 < \Delta E^* < 0.1\,{\rm GeV}$ and $5.27 < m_{\rm ES} < 5.29\,{\rm GeV}/c^2$. Selection criteria have been optimized for best $S^2/(S+B)$, where S and B are the expected signal and background yield assuming $\mathcal{B}[B^0 \to \rho^0\gamma] = \mathcal{B}[B^0 \to \omega\gamma] = \frac{1}{2}\mathcal{B}[B^+ \to \rho^+\gamma] = 10^{-6}$ (as expected from isospin symmetry) without knowledge of the yield or distribution of events in the signal region. The signal region extends lower on the negative side of ΔE^* due to the asymmetric photon energy response in the calorimeter resulting from energy leakage. For the small fraction of events (2.8 % for $B^0 \to \rho^0\gamma$ signal) in which more than one B meson candidate satisfies all the cuts, the candidate with the smallest value of $|\Delta E^*|$ is selected.

3.5 Suppression of Background

The continuum and initial state radiation backgrounds are suppressed by a neural network that combines event topology variables into one discriminating variable [9]. The neural network responds non-linearly to the input variables and exploits correlations between the variables. The input variables are:

- $\cos\theta_T^*$, the cosine of the angle between the photon and the thrust axis of the rest of the event (excluding the B meson candidate).
- $\cos\theta_B^*$, the cosine of the angle between the B meson momentum and the beam axis.
- The energy flow in 10° bins centered on the photon candidate momentum in the CMS.
- $\cos\theta_H$, the cosine of the helicity angle. For $B \to \rho\gamma$, we define θ_H as the angle between the π^+ momentum in the ρ rest frame and the ρ momentum in the B meson rest frame. For $B^0 \to \omega\gamma$, θ_H is defined as the angle between the normal to the plane defined by the $\pi^+\pi^-\pi^0$ momenta in the ω rest frame and the ω momentum in the B meson rest frame. $\cos\theta_H$ should follow a $\sin^2\theta_H$ distribution for signal, while the continuum background is approximately flat.
- R_2', the ratio of second and zeroth order Fox-Wolfram moments in the frame recoiling from the photon momentum. This is effective against initial-state radiation, since in that frame the jet structure of the hadrons is recovered.
- The net flavor content, defined as $\sum_i |N_i^+ - N_i^-|$, where $N_i^\pm$ are the number of $e^\pm$, $\mu^\pm$, $K^\pm$ and slow pions of each sign identified in the event.
- $|\Delta z|$, the vertex separation of the B meson candidate and the rest of the event along the beam axis, is used for $B^0 \to \rho^0\gamma$ and $B^0 \to \omega\gamma$.
- $\cos\theta_D$, the cosine of the Dalitz angle of the ω decay is used for $B^0 \to \omega\gamma$. $\cos\theta_D$ is defined as the angle between the. π^0 and the π^+ momenta in the rest frame of the $\pi^+\pi^-$ system. We expect $\cos\theta_D$ to be uniformly distributed for the combinatorial background and to follow a $\sin^2\theta_D$ distribution for true ω decays.

A separate neural network is trained for each mode using the back-propagation algorithm on samples of Monte Carlo-simulated signal and background. The output of the neural network, defined such that the signal processes peak at one and the continuum background at zero, is cross-checked on an independent sample of Monte Carlo-simulated events and data control samples for both the signal and background. The neural network output for $B^0 \to \rho^0\gamma$ is shown in Figure 2, where the Monte Carlo simulation of the continuum background is compared with the off-resonance data and the output for Monte Carlo-simulated $B^0 \to D^-\pi^+$ decays is compared with events reconstructed in the data. This latter check gives us confidence that the Monte Carlo simulates the $B \to \rho\gamma$ efficiency well, since most of the input variables of the neural network are not based on the properties of the signal decay itself, but rather on the properties of the other B meson in the event.

We make a selection on the neural network output optimized for best $S^2/(S+B)$ for each mode. For $B^+ \to \rho^+\gamma$, an additional requirement of $|\cos\theta_H| < 0.6$ is made to reject $B^+ \to \rho^+\pi^0$ events which have a $\cos^2\theta_H$ distribution, different from the expected $\sin^2\theta_H$ distribution from the signal process.

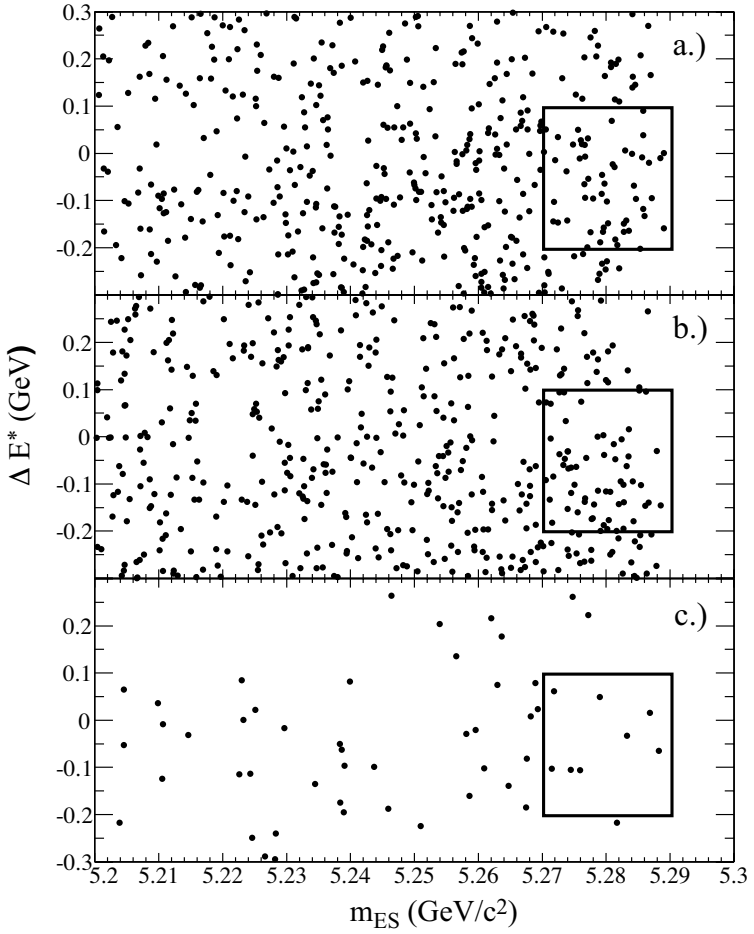

Figure 3: ΔE^* vs. $m_{\rm ES}$ for a.) $B^0 \to \rho^0\gamma$, b.) $B^+ \to \rho^+\gamma$ and c.) $B^0 \to \omega\gamma$ candidates.

3.6 Background Estimation

Table 1 shows estimates for the expected background remaining in the signal region ($-0.2 < \Delta E^* < 0.1\,\mathrm{GeV}$ and $m_{\rm ES} > 5.27\,\mathrm{GeV}/c^2$) after the neural network selection, using the off-resonance data for continuum and Monte Carlo simulation for $B\overline{B}$ backgrounds. There is good agreement between Monte Carlo estimates of continuum background and off-resonance data. The $B\overline{B}$ background is smaller than the continuum background.

3.7 Signal Extraction

After the neural network selection, the signal extraction in $B \to \rho\gamma$ is performed with an unbinned extended maximum likelihood fit in the variables $m_{\rm ES}$, ΔE^* and $M_{\pi\pi}$ with signal and continuum background components. Since the $B\overline{B}$ backgrounds are small relative to the continuum background, the signal extraction uses only a continuum component to describe the background. Biases due to $B\overline{B}$ backgrounds are estimated in the systematic studies described in Section 4. The signal $m_{\rm ES}$ and ΔE^* distributions are described by the Crystal Ball lineshape [11], with the exception of the $m_{\rm ES}$ distribution for $B^0 \to \rho^0\gamma$, where the Gaussian distribution is used. Here, we expect

	$B^0 \to \rho^0\gamma$	$B^+ \to \rho^+\gamma$	$B^0 \to \omega\gamma$
		(Events)	
Off-resonance data	42.8 ± 7.0	66.5 ± 8.8	7.3 ± 3.3
$uds + c\bar{c} + \tau^+\tau^-$ Monte Carlo	39.8 ± 3.8	59.8 ± 4.6	8.4 ± 1.9
$B\overline{B}$ Monte Carlo	6.6 ± 1.0	12.2 ± 3.6	0.7 ± 0.3
Signal Expectation	9.9 ± 0.2	12.1 ± 0.3	3.4 ± 0.1

Table 1: Estimates of continuum background (using both off-resonance data and Monte Carlo simulation), $B\overline{B}$ backgrounds and signal in the signal region. All estimates are scaled to a luminosity corresponding to 84 million $B\overline{B}$ pairs. Errors are statistical only.

the photon energy rescaling to eliminate the tail. The background $m_{\rm ES}$ and ΔE^* distributions are described by the ARGUS threshold function [12] and second order polynomial, respectively. For $B \to \rho\gamma$, the Breit-Wigner lineshape is used for the signal $M_{\pi\pi}$ distribution, while the background incorporates a sum of a resonant Breit-Wigner component and a continuum component described by a first order polynomial.

The parameters of the signal probability distributions are obtained from the Monte Carlo simulation and cross-checked in the data with the decays $B^0 \to K^{*0}\gamma$, $K^{*0} \to K^+\pi^-$ for $B^0 \to \rho^0\gamma$ and $B^+ \to K^{*+}\gamma$, $K^{*+} \to K^+\pi^0$ for $B^+ \to \rho^+\gamma$, which are topologically and kinematically similar. The parameters of the continuum background distributions are determined in the fit, with the exception of the fraction of the resonant $\rho \to \pi\pi$ contribution to the continuum $M_{\pi\pi}$ distribution, which is fixed to the value measured in the off-resonance data. In the $B^0 \to \omega\gamma$, the signal extraction is performed in a similar fit to the $m_{\rm ES}$ and ΔE^* distributions; the $M_{\pi^+\pi^-\pi^0}$ distribution is not included in the fit, because the continuum background contains a large and uncertain fraction of true ω decays, which is difficult to model.

By inverting the pion selection on the charged pion (and selecting kaons) in the $B^+ \to \rho^+\gamma$ analysis and on one of the charged pions in the $B^0 \to \rho^0\gamma$ analysis, we obtain an orthogonal sample of events enhanced in the decays $B^+ \to K^{*+}\gamma$, $K^{*+} \to K^+\pi^0$ and $B^0 \to K^{*0}\gamma$, $K^{*0} \to K^+\pi^-$, respectively. The yield of $B \to K^*\gamma$ in these two samples is determined using the same fit procedure described for $B \to \rho\gamma$, with the expected signal distributions determined from Monte Carlo simulation. The resulting yields are in agreement with the expectations from previous measurements of $\mathcal{B}[B \to K^*\gamma]$ [10], as shown in Table 2, thus providing a cross-check on the event selection and signal extraction procedure up to the statistical uncertainty in the extracted yields and the uncertainties in the measured branching fractions.

The ΔE^* vs. $m_{\rm ES}$ distributions of the $B \to \rho\gamma$ and $B^0 \to \omega\gamma$ candidates are shown in Figure 3 and the fitted yields summarized in Table 3. The quality of the fit is determined by comparing the minimum $-\log\mathcal{L}$ of the fit, where $\mathcal{L}$ is the overall likelihood of the fit, with values obtained from parameterized Monte Carlo simulation and found to be in good agreement.

4 Systematic Studies

The systematic uncertainties in this analysis are associated with uncertainties in the efficiency of the signal process reconstruction predicted by the Monte Carlo simulation and with the signal extraction procedure. Table 4 summarizes these uncertainties. The efficiency of the track selection is calculated by identifying tracks in the silicon vertex detector and evaluating the fraction that is

Mode	Fitted Yield (Events)	Expected Yield (Events)
$B^0 \to K^{*0}\gamma$	343.2 ± 21.0	332 ± 36
$B^+ \to K^{*+}\gamma$	93.1 ± 12.6	105 ± 18

Table 2: The fitted yields in the $B \to K^*\gamma$-enhanced sample described in the text, and the expected yield from the measured branching fractions in [10].

Mode	Yield (Events)	90% C.L. Upper Limit Yield (Events)	Bias (Events)	Efficiency (%)
$B^0 \to \rho^0\gamma$	4.8 ± 5.2	12.4	[-0.5,0.8]	12.3
$B^+ \to \rho^+\gamma$	6.2 ± 5.5	15.4	[-0.1,2.0]	9.2
$B^0 \to \omega\gamma$	0.1 ± 2.3	3.6	[-0.3,0.5]	4.6

Table 3: The fitted yields, the ranges of observed biases from $B\overline{B}$ backgrounds and selection efficiencies for $B^0 \to \rho^0\gamma$, $B^+ \to \rho^+\gamma$ and $B^0 \to \omega\gamma$ in the on-resonance data sample. The efficiencies include the branching fractions for $\omega \to \pi^+\pi^-\pi^0$ (88.8%), $\rho^0 \to \pi^+\pi^-$ ($\approx$ 99%) and $\rho^+ \to \pi^+\pi^0$ ($\approx$ 100%).

well-reconstructed in the drift chamber. The pion identification efficiency in the DIRC is derived from a sample of $D^{*+} \to D^0\pi^+, D^0 \to K^-\pi^+$ decays. The photon and π^0 efficiencies are measured by comparing the ratio of events $N(\tau^\pm \to h^\pm\pi^0)/N(\tau^\pm \to h^\pm\pi^0\pi^0)$, where $h^\pm = \pi^\pm, K^\pm$, to the previously measured branching ratios [13]. The photon isolation and π^0/η veto efficiency are dependent on the event multiplicity and are tested by "embedding" Monte Carlo-generated photons into both an exclusively reconstructed B meson data sample and a generic $B\overline{B}$ Monte Carlo sample. The efficiencies of the neural network selection are compared between the exclusively reconstructed $B \to D\pi$ events in the data and the Monte Carlo simulation of both the $B \to D\pi$ and signal processes, and the observed variations taken as systematic uncertainties. The $M_{\pi^+\pi^-\pi^0}$ selection for the $B^0 \to \omega\gamma$ is checked by comparing the resolution of the ω mass peak in the on-resonance data with the Monte Carlo simulation and evaluating the variation in efficiency.

Systematic uncertainties in the signal extraction procedure result from the modeling of the $B\overline{B}$ backgrounds and from uncertainties in the signal probability distribution functions used in the fit. The biases due to $B\overline{B}$ backgrounds are estimated by varying the distributions as well as the rates of the dominant backgrounds coming from $b \to s\gamma$ and $B^+ \to \rho^+\pi^0$ decays. The full range of biases obtained from these variations is taken as the allowed range, as shown in the column labeled "Bias" in Table 3. The uncertainties resulting from the fixed parameters describing the signal distributions in the fit are estimated by varying the parameters within the uncertainty obtained from the analogous $B \to K^*\gamma$ processes in the data used to cross-check the expectations from the Monte Carlo simulation. The effects of these variations on the fitted signal yield in each mode is calculated and the range of observed biases are taken as systematic uncertainties in the signal yield.

5 Physics Results

Based on the observed signal yields we determine 90% upper limits on the branching fraction by refitting the distributions with increasing fixed signal yields until the $-\log\mathcal{L}$ deviates by 0.82 relative to the minimum value. We correct for bias from $B\overline{B}$ backgrounds by applying the smallest observed

	$B^0 \to \rho^0\gamma$	$B^+ \to \rho^+\gamma$	$B^0 \to \omega\gamma$
	Systematic Uncertainty		
Selection Criteria	(%)	(%)	(%)
B Count	1.1	1.1	1.1
γ Eff.	1.5	1.5	1.5
π^0 Eff.	-	5.0	5.0
π^0/η Veto	1.0	1.0	1.0
γ Dist Cut	2.0	2.0	2.0
Tracking Eff.	2.5	1.3	2.4
π Selection	6.0	3.0	6.0
$M_{\pi^+\pi^-\pi^0}$ Selection	-	-	2.0
Neural network Selection	8.0	6.0	14.0
Fit Distributions	5.0	10.0	5.0
Total	11.8%	13.4%	17.3%

Table 4: Summary of systematic uncertainties for $B \to \rho\gamma$ and $B^0 \to \omega\gamma$ expressed as percent error of the branching fraction.

bias to the signal yield (increasing the signal yield in all cases). The yield of events in the data sample are calculated with the Monte Carlo-derived efficiency lowered by one standard deviation in the systematic error. Finally, the estimated number of $B\overline{B}$ events in the sample is reduced by one standard deviation. The resulting preliminary 90% confidence level upper limits for the branching fractions are $\mathcal{B}[B^0 \to \rho^0\gamma] < 1.4 \times 10^{-6}$, $\mathcal{B}[B^+ \to \rho^+\gamma] < 2.3 \times 10^{-6}$ and $\mathcal{B}[B^0 \to \omega\gamma] < 1.2 \times 10^{-6}$.

For the purpose of comparing the limits to $\mathcal{B}[B \to K^*\gamma]$, we combine these limits into a single limit on the generic process $B \to \rho\gamma$ defined as

$$\mathcal{B}[B \to \rho\gamma] \equiv \mathcal{B}[B^+ \to \rho^+\gamma] = 2 \times \mathcal{B}[B^0 \to \rho^0\gamma] = 2 \times \mathcal{B}[B^0 \to \omega\gamma].$$

as expected from isospin symmetry. The resulting preliminary 90% confidence level upper limit is $\mathcal{B}[B \to \rho\gamma] < 1.9 \times 10^{-6}$. Using the measured value of $\mathcal{B}[B \to K^*\gamma]$ [10], this corresponds to a ratio of

$$\mathcal{B}[B \to \rho\gamma]/\mathcal{B}[B \to K^*\gamma] < 0.047.$$

We can convert this ratio to a limit on $|V_{td}/V_{ts}|$ using the following expression from [3].

$$\frac{\mathcal{B}[B \to \rho\gamma]}{\mathcal{B}[B \to K^*\gamma]} = \left|\frac{V_{td}}{V_{ts}}\right|^2 \left(\frac{1 - m_\rho^2/M_B^2}{1 - m_{K^*}^2/M_B^2}\right)^3 \zeta^2[1 + \Delta R].$$

Taking the conservative limits of the two parameters, $\zeta = 0.7$ and $\Delta R = -0.25$, we find $|V_{td}/V_{ts}| < 0.36$ at 90% Confidence Level.

6 Summary

In conclusion, we have found no evidence for the exclusive $b \to d\gamma$ transitions $B \to \rho\gamma$ and $B^0 \to \omega\gamma$ in 84 million $B\overline{B}$ decays studied with the *BABAR* detector. The preliminary 90% confidence level upper limits on the branching fractions are significantly improved and within a factor of two of the largest Standard Model predictions, which indicate a range $\mathcal{B}[B^+ \to \rho^+\gamma] = (0.9 - 1.5) \times 10^{-6}$.

7 Acknowledgments

We are grateful for the extraordinary contributions of our PEP-II colleagues in achieving the excellent luminosity and machine conditions that have made this work possible. The success of this project also relies critically on the expertise and dedication of the computing organizations that support *BABAR*. The collaborating institutions wish to thank SLAC for its support and the kind hospitality extended to them. This work is supported by the US Department of Energy and National Science Foundation, the Natural Sciences and Engineering Research Council (Canada), Institute of High Energy Physics (China), the Commissariat à l'Energie Atomique and Institut National de Physique Nucléaire et de Physique des Particules (France), the Bundesministerium für Bildung und Forschung and Deutsche Forschungsgemeinschaft (Germany), the Istituto Nazionale di Fisica Nucleare (Italy), the Research Council of Norway, the Ministry of Science and Technology of the Russian Federation, and the Particle Physics and Astronomy Research Council (United Kingdom). Individuals have received support from the A. P. Sloan Foundation, the Research Corporation, and the Alexander von Humboldt Foundation.

References

[1] See for example, S. Bertolini, F. Borzumati and A. Masiero, Nucl. Phys. B **294**, 321 (1987); H. Baer, M. Brhlik, Phys. Rev. D **55**, 3201 (1997); J. Hewett and J. Wells, Phys. Rev. D **55**, 5549 (1997); M. Carena *et al.*, Phys. Lett. B **499**, 141 (2001).

[2] M. Beneke, T. Feldmann and D. Seidel, Nucl. Phys. B **612**, 25 (2001); S. W. Bosch and G. Buchalla, Nucl. Phys. B **621**, 459 (2002).

[3] A. Ali and A. Y. Parkhomenko, Eur. Phys. J. C **23**, 89 (2002).

[4] B. Grinstein and D. Pirjol, Phys. Rev. D **62**, 093002 (2000).

[5] CLEO Collaboration, T.E. Coan *et al.*, Phys. Rev. Lett. **84**, 5283 (2000); BELLE Collaboration, Y. Ushiroda *et al.*, contributed to BCP4, Ago Town, Japan, Feb 2001. hep-ex/0104045.

[6] BABAR Collaboration, B. Aubert *et al.*, Nucl. Instrum. Meth. A **479**, 1 (2002).

[7] PEP-II Conceptual Design Report, SLAC-0418 (1993).

[8] Geant4 Collaboration, "Geant4 - A Simulation ToolKit", CERN-IT-2002-003. To be published in Nucl. Instrum. Meth. A.

[9] We use the Stuttgart Neural Network Simulator:
http://www-ra.informatik.uni-tuebingen.de/SNNS

[10] BABAR Collaboration, B. Aubert *et al.*, Phys. Rev. Lett. **88**, 101805 (2002).

[11] The "Crystal Ball" lineshape is a modified Gaussian distribution with a transition to a tail function on one side: $f_{CB} = \exp -\frac{(x-\mu)^2}{2\sigma^2}$ for $\frac{x-\mu}{\sigma} > \alpha$ and $A \times [B - (\frac{x-\mu}{\sigma})^{-n}]$ for $\frac{x-\mu}{\sigma} < \alpha$ where $A \equiv (\frac{n}{\alpha})^n \exp -\frac{1}{2}|\alpha|^2$ and $B \equiv \frac{n}{\alpha} - |\alpha|$ are defined such as to maintain continuity of the function and its first derivative.

[12] We use the distribution $x\sqrt{1-x^2} \times \exp[\zeta(1-x^2)]$, where $x = m_{\rm ES}/E^*_{beam}$, to describe the background $m_{\rm ES}$ distribution. The function was introduced by the ARGUS collaboration; H.Albrecht *et al.*, Z. Phys. C **48**, 543 (1990)

[13] CLEO Collaboration, M. Procario *et al.*, Phys. Rev. Lett. **70**, 1207 (1993).